Peculiar atomic dynamics in liquid GeTe with asymmetrical bonding: Observation by inelastic x-ray scattering

M. Inui,[1,*] A. Koura,[2] Y. Kajihara,[1] S. Hosokawa,[2] A. Chiba,[3] K. Kimura,[4,†] F. Shimojo,[2] S. Tsutsui,[5] and A. Q. R. Baron[6]

[1]*Graduate School of Integrated Arts and Sciences, Hiroshima University, Higashi-Hiroshima, Hiroshima 739-8521, Japan*

[2]*Department of Physics, Kumamoto University, Kumamoto 860-8555, Japan*

[3]*Department of Physics, Keio University, Yokohama 223-8522, Japan*

[4]*Graduate School of Science, Kyoto University, Kyoto 606-8502, Japan*

[5]*Japan Synchrotron Radiation Research Institute (JASRI), Sayo, Hyogo 679-5198, Japan*

[6]*Materials Dynamics Laboratory, RIKEN SPring-8 Center, Sayo, Hyogo 679-5148, Japan*

(Received 14 May 2017; revised manuscript received 28 February 2018; published 14 May 2018)

Collective dynamics in liquid GeTe was investigated by inelastic x-ray scattering at $2 \leqslant Q \leqslant 31$ nm^{-1}. The dynamic structure factor shows clear inelastic excitations. The excitation energies at low Q disperse with increasing Q, consistent with the behavior of a longitudinal-acoustic excitation. The dispersion curve has a flat-topped region around the pseudo-Brillouin-zone boundary, similar to what is observed in liquid Bi [Inui *et al.*, Phys. Rev. B **92**, 054206 (2015)]. The dynamic structure factor shows a low-frequency excitation, and its coupling with the longitudinal-acoustic mode plays an important role for a flat-topped dispersion. From these results, it is inferred that atomic dynamics in liquid GeTe is strongly affected by a Peierls distortion similar to liquid Bi. By comparing the momentum transfer dependence of the excitation energy and quasielastic linewidth to partial structure factors obtained by our own *ab initio* molecular dynamics simulation for liquid GeTe, the quasielastic and inelastic components were found to be correlated with Te-Te and Ge-(Ge,Te) partial structure factors, respectively.

DOI: 10.1103/PhysRevB.97.174203

I. INTRODUCTION

Studies on atomic dynamics in binary liquids are a subject of great interest owing to their increased degrees of freedom compared to those in monatomic liquids. In particular, fast sound and an optical mode have been topics of interest. A fast sound phenomenon appears in binary fluids and liquids with large difference in particle mass, where a high-frequency collective motion of lighter particles is bifurcated from normal collective motions [1–3]. Although inelastic neutron scattering (INS) experiments of liquid Li_4Pb and Li_4Tl [4] confirmed high-frequency excitations in the dynamic structure factors $S(Q,E)$, where Q and E are momentum and energy transfer, respectively, the possible merging of the fast sound with the hydrodynamic sound mode was not determined due to a lack of data at low Q. A molecular dynamics (MD) study combined with the generalized collective mode (GCM) approach reported that the low-frequency hydrodynamic acoustic modes without any fast sound define the Brillouin peak at $Q \sim 4$ nm^{-1} in liquid Li_4Tl, whereas the high-frequency modes mainly contribute to the side peak of $S(Q,E)$ for $Q > 4$ nm^{-1} [5]. Meanwhile, an optical mode was predicted by theoretical work on one component plasma [6]. $S(Q,E)$ simulated at approximately $0.15Q_p$ [Q_p is the first peak position in the structure factor $S(Q)$] exhibited a distinct excitation near an ionic plasma frequency similarly to that in an ionic solid. MD simulations were carried out to study an optical mode in a number of molten salts [7–9]. To confirm an optical mode in real molten salts, inelastic neutron scattering (INS) [10–12] was carried out but could not obtain the data at low Q where a distinct optical mode is expected. Recently, excitations of an optical mode at small Q values were shown to be very tiny by an *ab initio* molecular dynamics (AIMD) simulation [13]. As predicted by the AIMD, inelastic x-ray scattering (IXS) spectra of molten NaI showed small and damped excitations of longitudinal-optic-phonon modes at the tail of the longitudinal-acoustic modes [14].

It is also interesting to consider liquid GeTe from the point of view of a Peierls distortion. Solid GeTe has an $A7$ crystalline form (in Strukturbericht symbols) where distortion changes the six isotropic bonds in the rocksalt structure into three shorter and three longer bonds. Thus an $A7$ crystalline structure type is understood as a three-dimensional Peierls distortion: Peierls [15] predicted that a regular metallic chain is unstable for a distortion and dimerization occurs to gain electronic energy by generating a gap in a metallic band. Asymmetrical bonding originating from the Peierls distortion was found by a neutron diffraction (ND) [16] for liquid As that has an A7 crystalline form in a solid state. From ND and AIMD simulation results for liquid GeTe, Raty *et al.* [17] reported the average first-nearest coordination number approaching 3 with decreasing temperature, the bond angle distributions exhibiting a maximum at approximately 90°, and the angular limited triplet correlation indicating alternation of shorter and longer bonds, and they strongly suggested that the Peierls distortion is

*masinui@hiroshima-u.ac.jp

†Present address: Nagoya Institute of Technology, Nagoya, Aichi 466-8555, Japan.

realized as asymmetrical bonding in liquid GeTe. Alternatively, as GeTe is a prototype of phase-change materials utilized for data storage devices, properties in the liquid and supercooled liquid states are interesting. From this point of view, structural, viscous, and electronic properties of liquid GeTe have been studied by means of x-ray and neutron-diffraction experiments and AIMD simulations [18].

Because liquid GeTe is a system where the Peierls distortion and asymmetrical bonding are expected, we were prompted to study collective dynamics in this liquid. We have measured IXS spectra of liquid GeTe to investigate the acoustic excitations in $S(Q,E)$. The IXS technique has an advantage for the measurements at extreme conditions at high temperatures and high pressures owing to high brilliant incident beam of < 0.1 mm diameter. Using our technique to keep a thin liquid slab stable and an excellent spectrometer system [19] at SPring-8 in Japan, we could obtain IXS spectra with good statistics.

We analyzed the IXS data of liquid GeTe using a model function based on the interacting oscillators as done for liquid Zn [20,21], and found that $S(Q,E)$ exhibits a low-energy excitation below a longitudinal-acoustic excitation. The peak energy of the current-current correlation function in liquid GeTe shows a flat-topped dispersion curve as a function of Q. As the longitudinal-acoustic excitations in liquid Bi are reported to exhibit a flat-topped dispersion curve [22,23], we reanalyzed the IXS data of liquid Bi using the same model function of the interacting oscillators. The results suggest that a coupling between a longitudinal-acoustic and low-frequency modes is important to explain a peculiar dispersion curve in these liquids. To analyze the experimental results of liquid GeTe more deeply, we used partial structure factors obtained by our own AIMD simulation for liquid GeTe [24]. As a result, we found that the excitation energy of the acoustic mode is related to the partial dynamic structure factors of Ge-Ge and Ge-Te while the quasielastic excitations are dominated by that of Te-Te.

This paper is organized as follows. After describing our experimental procedure and simulation method, we present IXS results in Sec. IV. In Sec. V, we describe partial structures and single-particle dynamics obtained by AIMD simulations, and discuss collective dynamics in liquid GeTe, comparing to the results in liquid Bi. Then the present results are summarized in Sec. VI.

II. EXPERIMENTAL PROCEDURE

The IXS experiments were conducted at the high-resolution IXS beamline (BL35XU) of SPring-8 in Japan [19]. Backscattering at the Si (11 11 11) reflection provided a beam of approximately 10^{10} photons/sec in a 0.8-meV bandwidth onto the sample. The energy of the incident beam and the Bragg angle of the backscattering were 21.747 keV and approximately 89.98°, respectively. We used 12 spherical analyzer crystals at the end of the 10-m horizontal arm. The spectrometer resolution was approximately 1.5 meV depending on each analyzer crystal, as was determined by measurements of polymethyl methacrylate (PMMA). The Q resolution, ΔQ, was set to be 0.45 and 1.0 nm^{-1} (full width) for $Q \leqslant 11$ and $Q > 11$ nm^{-1}, respectively.

The GeTe sample of 99.999% purity and 0.16 mm thickness was mounted in a single-crystalline sapphire Tamura-type cell [25] which was placed in a high-pressure vessel. The vessel was filled with He gas (99.999% purity) at 1 MPa to stabilize the liquid state. The sample thickness was determined using the density [26] to give a proper optical thickness for the incident x-ray. IXS spectra of liquid GeTe in a cell and the background using an empty cell were measured at 1073 K. Further information on the setup of IXS experiments using high-pressure gas apparatus is described in [27]. After background subtraction with the absorption correction and integration with respect to E, we deduced the normalized dynamic structure factor $S(Q,E)/S(Q)$ of liquid GeTe from these spectra.

III. METHOD OF CALCULATION

The electronic states were calculated using the projector-augmented-wave (PAW) method within the framework of the density-functional theory (DFT) in which the generalized gradient approximation (GGA) was used for the exchange-correlation energy. Projector functions of the s, p, and d types were generated for the $4s$, $4p$, and $4d$ states of Ge, and the $5s$, $5p$, and $5d$ states of Te. The plane-wave cutoff energies were 9 and 90 Ry for the electronic pseudowave functions and the pseudocharge density, respectively. The energy functional was minimized using an iterative scheme [28,29]. The Γ point was used for Brillouin-zone sampling.

Molecular dynamics simulations were carried out for the system of 128 atoms (Ge:64, Te:64) in a cubic supercell under periodic boundary condition. Using the Nosé-Hoover thermostat, the equations of motion were solved via an explicit reversible integrator with a time step of $\Delta t = 2.90$ fs. The quantities of interest were obtained by averaging over 24.7 ps after an initial equilibration taking at least 1.45 ps. The temperature T was 1000 K and the number density ρ (=29.9 nm^{-3}) was obtained by 2000 MD steps of the isothermal-isobaric ensemble. The ρ agrees approximately with the experimentally determined 33.3 nm^{-3} [26]. This density difference of approximately 10% did not make a critical influence on main results discussed in this paper. Detailed results of this simulation are presented in [24].

IV. RESULTS

Figure 1 shows $S(Q,E)/S(Q)$ of liquid GeTe at 1073 K. $S(Q,E)/S(Q)$ at 2.0 nm^{-1} exhibits the inelastic excitation at ± 2.4 meV on both sides of the central quasielastic peak. The inelastic excitation is visible up to 15.9 nm^{-1}, and disperses with increasing Q at $Q \leqslant 11.9$ nm^{-1}. As Q approaches 20 nm^{-1} from below, the inelastic excitations become small and the central quasielastic component becomes dominant. 20 nm^{-1} is close to Q_p in liquid GeTe. $S(Q,E)/S(Q)$ at $Q \geqslant 22.6\,\mathrm{nm}^{-1}$ exhibits a characteristic profile: it is difficult to distinguish inelastic excitations clearly from the central peak.

We plot E integration of $S(Q,E)$ as a function of Q by open squares in Fig. 2. The integration corresponds to the scattering intensity $F(Q)$ defined by

$$F(Q) = \langle f \rangle^2 S(Q) + \langle f^2 \rangle - \langle f \rangle^2, \tag{1}$$

where f and $\langle\ \rangle$ are the atomic form factor cited from [30] and a molar fraction average, respectively. $F(Q)$ was calculated

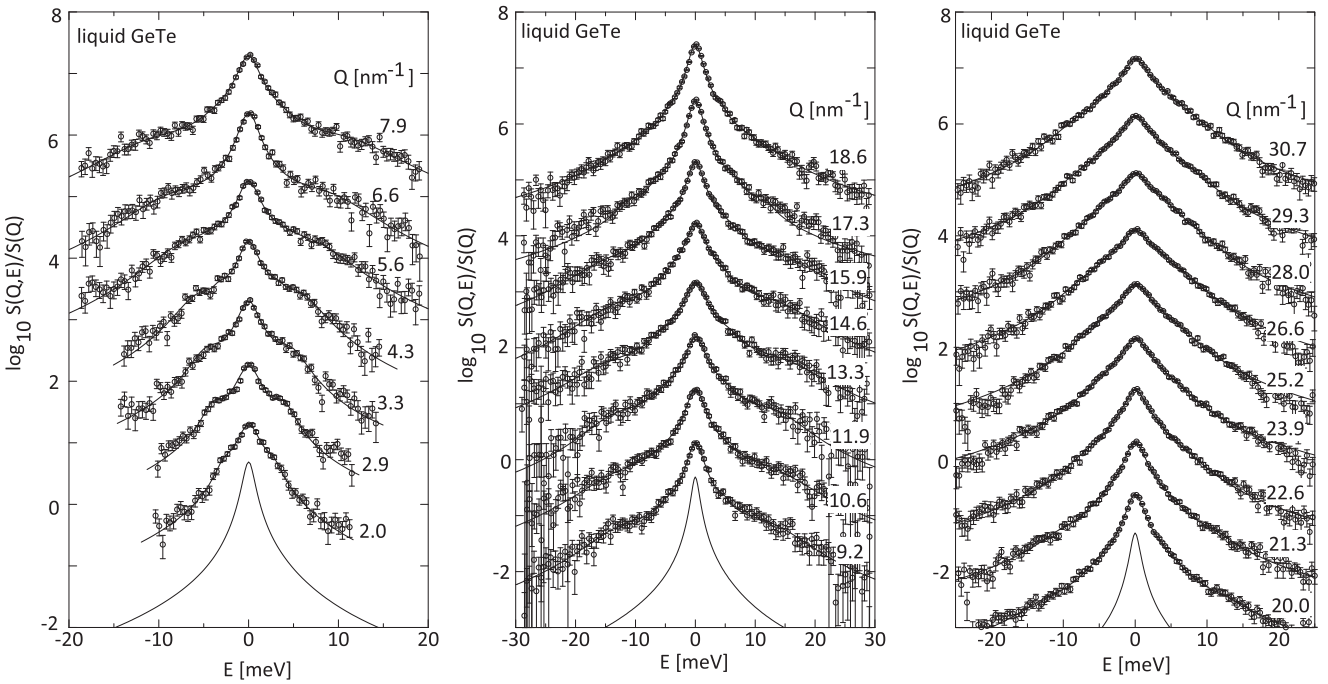

FIG. 1. $S(Q,E)/S(Q)$ of liquid GeTe at 1073 K. Open circles and solid lines denote the experimental results and the optimized fits with the model function, respectively. Each spectrum is shifted by multiplying 10 for clarity. Q values are shown in the right-hand side. The resolution function is shown by a solid line at the bottom. Scan ranges at low Q were limited to conserve beam time.

using $S_{\mathrm{XD}}(Q)$ obtained by x-ray diffraction (XD) by Kohara *et al.* [31] and it is denoted by brown dots in the figure. The open squares were normalized to the brown dots at 6 nm^{-1}. The IXS data agree well with brown dots at $Q < 19\ \mathrm{nm}^{-1}$ whereas the integration at 21 nm^{-1} lies at a position lower than the peak intensity of $F(Q)$. The integration at 32 nm^{-1} is also smaller than $F(Q)$. These Q positions were measured by the same three analyzers arranged on the fourth vertical line, and the adjustment of the collimation system makes the receiving efficiency for scattered x rays on the fourth line more sensitive to the sample position than the remaining nine analyzers arranged at lower scattering angles. Hence we suppose that a small deviation of the sample position along the incident x ray from the center of the goniometer made this disagreement at high Q while the wrong sample position gave no effect at small scattering angles corresponding to $Q \leqslant 16\ \mathrm{nm}^{-1}$. The figure also shows $F(Q)$ obtained by our AIMD simulation $S_{\mathrm{AIMD}}(Q)$. $S_{\mathrm{AIMD}}(Q)$ is compared to $S_{\mathrm{XD}}(Q)$ in the inset. These structure factors reasonably agree with each other but effects of the density difference are observable as a small phase shift at $Q \geqslant 30\ \mathrm{nm}^{-1}$.

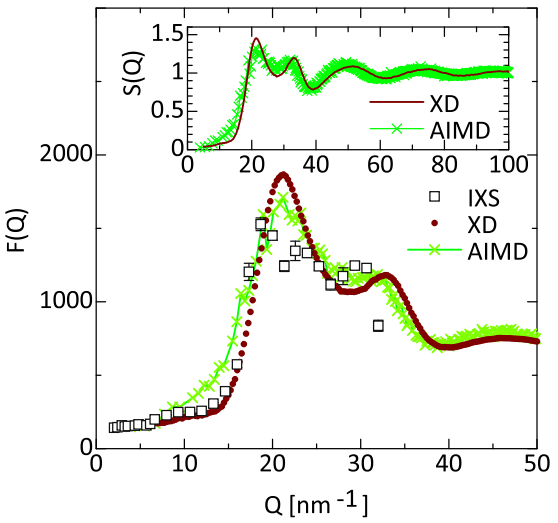

FIG. 2. The integration of $S(Q,E)$ normalized at 6 nm^{-1} to $F(Q)$ obtained by $S_{\mathrm{XD}}(Q)$ [31] is denoted by brown dots. Also shown is $F(Q)$ obtained by $S_{\mathrm{AIMD}}(Q)$. The inset shows $S_{\mathrm{XD}}(Q)$ at 1073 K [31] and $S_{\mathrm{AIMD}}(Q)$ at 1000 K.

We deconvoluted the experimental $S(Q,E)/S(Q)$ of liquid GeTe using the resolution function $R(E)$ and a model function $F_{\mathrm{m}}(Q,E)$ consisting of a Lorentzian for the quasielastic peak and a function of a system of two interacting oscillators for the inelastic excitation [21,32,33], in order to represent a low-energy excitation arising from a transverse-acoustic excitation in the longitudinal-acoustic correlation function. The model function is expressed by

$$S(Q,E)/S(Q) = \int dE'[F_{\mathrm{m}}(Q,E')]R(E-E'), \quad (2)$$

$$F_{\mathrm{m}}(Q,E) = B(E)\frac{A_0}{\pi}\frac{\Gamma_{\mathrm{L}}}{\Gamma_{\mathrm{L}}^2+E^2} + [1+n(E)]\sum_{j=1}^{2} A_j \mathrm{Im}[G_{jj}(Q,E)],$$

$$G_{jj}(Q,E) = \frac{1}{2\pi}\frac{\chi_j(Q,E)}{1-\chi_1(Q,E)\chi_2(Q,E)|U(Q)|^2},$$

$$\chi_j(Q,E) = \left[E^2-\omega_j^2-iE\Gamma_j\right]^{-1},$$

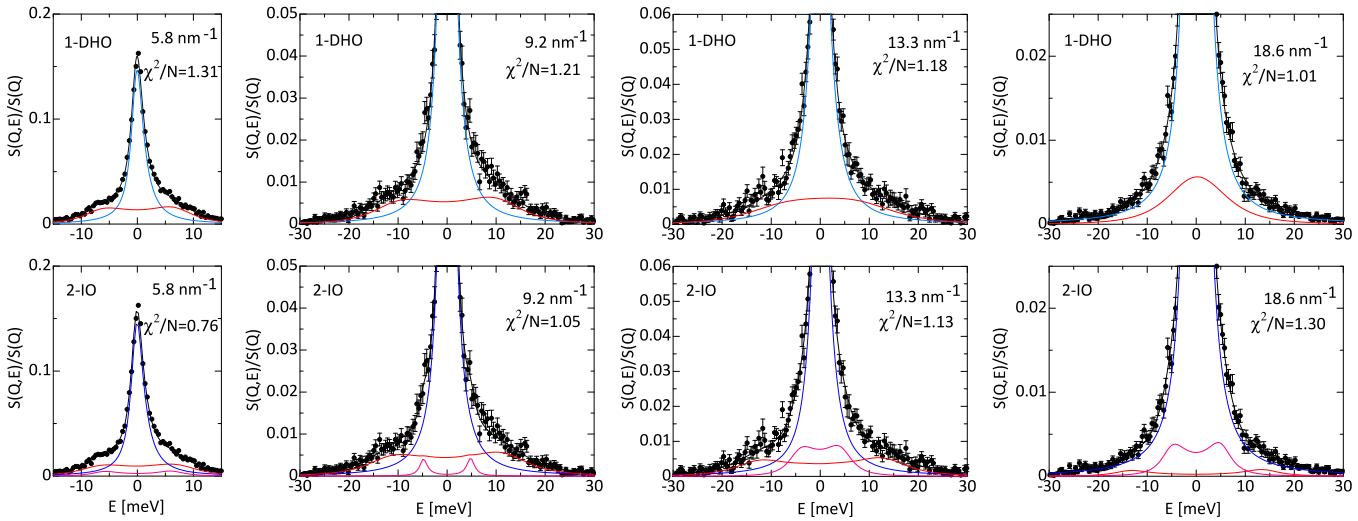

FIG. 3. $S(Q,E)/S(Q)$ of liquid GeTe. Circles denote IXS results and solid curves indicate the best fits. Upper and lower panels denote the results of 1-DHO and interacting oscillators (2-IO), respectively. The quasielastic and inelastic components are denoted by blue, red, and magenta lines, respectively.

$$B(E) = \beta E/[1-\exp(-\beta E)],$$
$$1+n(E) = 1/[1-\exp(-\beta E)], \quad (3)$$

where $\beta = (k_B T)^{-1}$. A_0 and Γ_L are the amplitude and linewidth of Lorentzian, respectively. A_j, Γ_j, and ω_j are the amplitude, linewidth, and excitation energy for the jth oscillator, respectively. For the coupling parameter between $j=1$ and $j=2$, $U(Q) \neq 0$, two oscillators are interacted and $\mathrm{Im}[G_{jj}(Q,E)]$ exhibits two maxima at around ω_1 and ω_2. We imposed a condition of $\Gamma_j < \omega_j$, similarly to a damped harmonic oscillator model [34]. We abbreviate this model function as 2-IO (two interacting oscillators). Because we will later compare ω_j with that of liquid Bi, we also carried out the same analysis as used for the liquid-Bi data presented in [23].

We carried out deconvolution of $S(Q,E)/S(Q)$ at all Q with 2-IO. We also carried out deconvolution using a model function consisting of a Lorentzian and a damped harmonic oscillator function [34]. To show that the second excitation energy is needed, we compared the results with the fits using a Lorentzian and one damped harmonic oscillator function (1-DHO) and two damped harmonic oscillator functions (2-DHO). Figure 3 shows $S(Q,E)/S(Q)$ at 5.8, 9.2, 13.3, and 18.6 nm^{-1} with the components of the model functions. χ^2 per a degree of freedom, χ^2/N, is indicated in each panel. $S(Q,E)/S(Q)$ was well reproduced by 2-IO and χ^2/N indicates that 2-IO gave better fits than 1-DHO. Although χ^2/N of 1-DHO is better than 2-IO at 18.6 nm^{-1}, 2-IO is proper as described in the next paragraph.

To select a proper model function, we carried out Bayesian analysis [20,35] for 1-DHO, 2-DHO, and 2-IO. Figure 4 shows a proper model for each spectrum selected by a posterior ratio among these model functions. Bayesian analysis shows that 2-IO is superior to the others besides several spectra. A gap between 21 and 28 nm^{-1} means that Bayesian analysis does not work well probably because the acoustic excitation is strongly damped at these Q positions. 2-IO results are accepted at almost every Q except for $21 \leqslant Q \leqslant 28$ nm^{-1}. As the excitation energies were not largely different between 2-IO and 2-DHO, hereafter we discuss atomic dynamics using the 2-IO results.

ω_1 and ω_2 are shown by light blue circles and triangles, respectively, in Fig. 5. Also shown is a peak position (ω_{pk}) of the current-current correlation function $[E^2 F_m(Q,E)/Q^2]$ calculated using the deconvoluted model function by black squares. The black squares disperse along the sound speed of 2200 m/s, which is 43% faster than the ultrasonic sound speed of 1530 m/s [26]. The linear dependence at low Q suggests that the excitation originates from a longitudinal-acoustic mode. The strength of positive dispersion, 43%, is larger than the normal values of 10–20% in simple liquid metals, similar to the large positive value of 34% obtained for liquid Bi. The black squares exhibit a flat-topped profile similar to that in liquid Bi reported in Ref. [23]. ω_2 at low Q is scattered and it stays at $4 \leqslant E \leqslant 7$ meV at $Q \geqslant 8$ nm^{-1}.

Figure 6 shows the linewidth parameters Γ_1 (light blue circles) and Γ_2 (light blue triangles). Γ_1 and Γ_2 at low Q

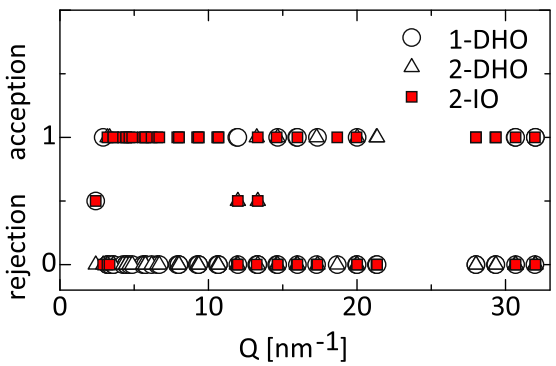

FIG. 4. A proper model for each spectrum measured by 12 analyzer crystals determined by Bayesian analysis. The symbols superimposed at 1.0 mean that Bayesian analysis suggests different models at the Q where three or two independent spectra are obtained. The symbols at 0.5 mean that posterior ratios for the spectrum are almost the same values between these models.

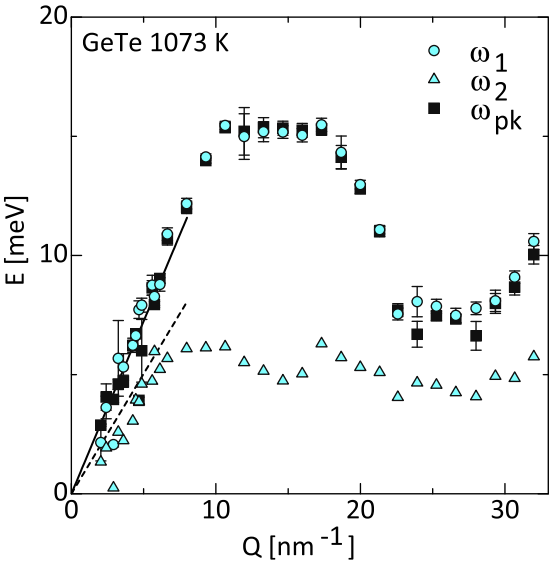

FIG. 5. Q dependence of ω_1, ω_2, and ω_{pk} obtained by 2-IO at $Q \geqslant 2$ nm^{-1}. Solid and broken lines denote the dispersion of 2200 m/s and the ultrasonic sound speed, respectively.

show approximately Q^2 dependence although the optimized Γ_2 are scattered. From Γ_2 as high as ω_2 at $Q \geqslant 10$ nm^{-1}, it is inferred that the low-energy excitation is nearly overdamped at the pseudo-Brillouin-zone boundary.

V. DISCUSSION

A. Partial structure factors

We discuss the partial structure factors of liquid GeTe obtained by our own AIMD. Figure 7 shows the partial pair distribution functions $g_{\alpha\beta}(r)$ ($\alpha,\beta =$ Ge, Te) in liquid GeTe. $g_{\mathrm{GeGe}}(r)$ and $g_{\mathrm{GeTe}}(r)$ exhibit a distinct peak at the first

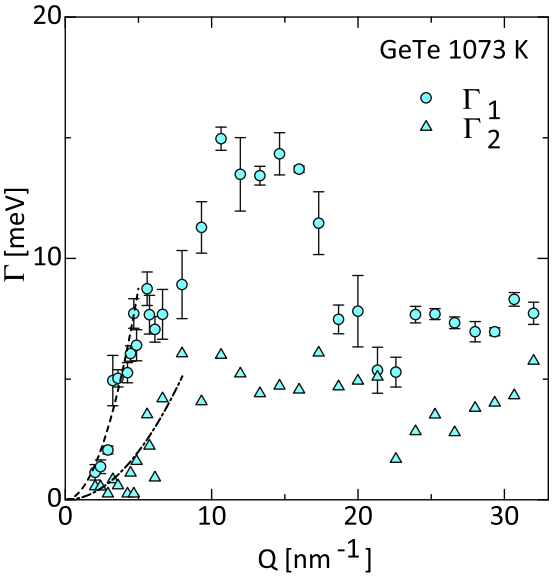

FIG. 6. Q dependence of Γ_1 and Γ_2 obtained by 2-IO at $Q \geqslant 2$ nm^{-1}. The broken and chain curves denote Q^2 dependence for a guide of reader's eyes.

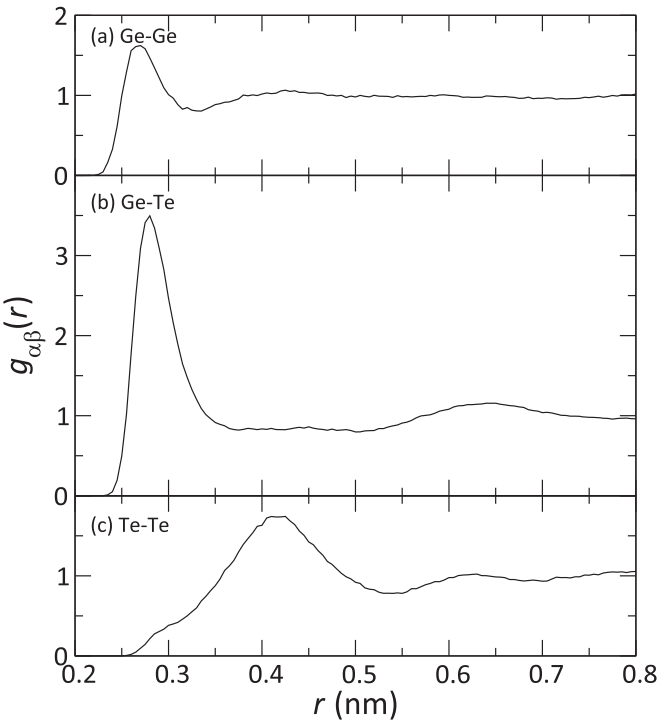

FIG. 7. Partial pair distribution functions, $g_{\alpha\beta}(r)$ ($\alpha,\beta =$ Ge, Te), of (a) Ge-Ge, (b) Ge-Te, and (c) Te-Te pairs in liquid GeTe obtained by the present AIMD.

coordination shell whereas $g_{\mathrm{TeTe}}(r)$ has a broad maximum at approximately 0.42 nm. These results indicate that the population of Te-Te bonds at the first coordination shell is smaller compared to those of "Ge-Ge" and "Ge-Te" bonds. $g_{\mathrm{GeGe}}(r)$ previously reported [17] exhibits the first peak as sharp as that in $g_{\mathrm{GeTe}}(r)$. The result is different from the broad first peak in $g_{\mathrm{GeGe}}(r)$ presented here. However, as shown in Table I, the partial coordination numbers with the same cutoff distance (r_c) are not very different between each other. Further, our results seem to agree well with the partial coordination numbers obtained by another AIMD simulation [18] when the difference of r_c is corrected. To confirm consistency among these AIMD simulations, we investigated an angular-limited triplet correlation in the atomic configurations obtained by our AIMD, and found that alternation of shorter and longer bonds as realized, as reported in Refs. [17,18]. This result suggests that the Peierls distortion is stabilized in liquid GeTe. As indicated in Table I, when the cutoff distance (r_c) of 0.3 nm corresponding to a shorter bond was taken, the partial coordination numbers of Ge-Ge (N_{GeGe}) and Ge-Te (N_{GeTe}) pairs were approximately 1.1 and 1.9, respectively, whereas the number of a Te-Te pair (N_{TeTe}) was 0.1. The total coordination numbers at Ge (N_{Ge}) and Te (N_{Te}) sites were 3.0, and 2.0, respectively. N_{Te} became approximately 3 when $r_c = 0.32$ nm was taken. These results also support stabilization of the Peierls distortion. Thus our AIMD results were mostly consistent with the previous ones [17,18] although our results predicted slightly fewer homopolar bonds than Ref. [17].

Figure 8 shows bond angle distributions of Ge-Te-Ge and Te-Ge-Te triplets. The Te-Ge-Te distribution obtained by

TABLE I. Total and partial coordination numbers for a cutoff distance r_c in liquid GeTe.

T (K)	N_{GeGe} [r_c (nm)]	N_{GeTe} [r_c (nm)]	N_{TeTe} [r_c (nm)]	N_{Ge}	N_{Te}	N
1000	1.085 (0.30)	1.915 (0.30)	0.132 (0.30)	3.001	2.047	2.524
1000	1.423 (0.32)	2.595 (0.32)	0.300 (0.32)	4.017	2.896	3.457
1000	1.961 (0.348)	3.259 (0.348)	0.704 (0.348)	5.167	3.962	4.565
1000 [17]	2.56(9) (0.348)	2.87(9) (0.348)	1.11(9) (0.348)	5.43(19)	3.98(18)	4.70(19)
1032 [18]	1.21 (0.318)	2.95 (0.332)	0.48 (0.340)	4.16	3.43	3.80

$r_c = 0.30$ nm corresponding to shorter bonds exhibits a sharp maximum at approximately 98° consistent with the bond angle in the $A7$ crystalline form, while the Ge-Te-Ge distribution is broader than the Te-Ge-Te one and exhibits a maximum at 90°. This result indicates that Ge atoms favor a local order of the $A7$ crystalline form compared to Te atoms. When $r_c = 0.32$ nm is taken, the maximum in the Te-Ge-Te distribution shifts to an angle slightly smaller than 98° while the Ge-Te-Ge distribution is slightly broadened.

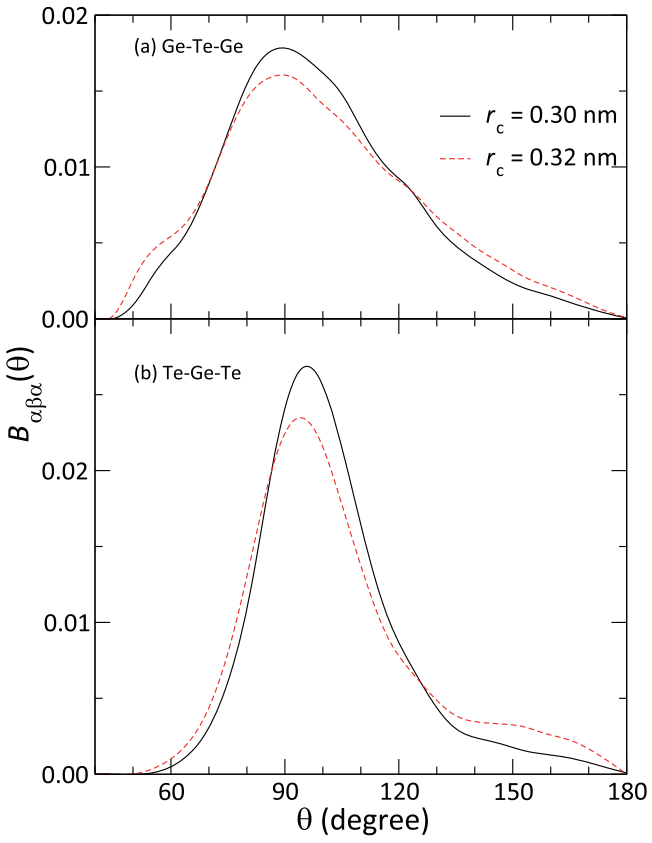

FIG. 8. Bond angle distributions for heteropolar bonds (a) at a Te site and (b) at a Ge site in liquid GeTe obtained by the present AIMD simulation. Solid and broken lines denote the distribution of the cutoff distances of 0.30 and 0.32 nm, respectively.

Figure 9 shows the partial structure factors $S_{\alpha\beta}(Q)$ obtained by our AIMD. The first maximum in $S_{\mathrm{XD}}(Q)$ stays at 21 nm^{-1}. The maxima of $S_{\mathrm{GeGe}}(Q)$ and $S_{\mathrm{GeTe}}(Q)$ shift to Q higher than 21 nm^{-1} whereas that of $S_{\mathrm{TeTe}}(Q)$ shifts to lower Q. The second maximum in $S_{\mathrm{XD}}(Q)$ mainly comes from that in $S_{\mathrm{TeTe}}(Q)$. In Sec. V C, we utilized $S_{\alpha\beta}(Q)$ to discuss collective dynamics in liquid GeTe.

B. Single-particle dynamics

Figure 10 shows the velocity autocorrelation functions $\phi_\alpha(t)$ and its power spectra $\bar{\phi}_\alpha(\omega)$, where α denotes Ge or Te. $\phi_{\mathrm{Ge}}(t)$ shows a profile of damping oscillations including a backflow process. In contrast, $\phi_{\mathrm{Te}}(t)$ is strongly damped without a backflow one. There appear two maxima at approximately 3 and 16 meV in $\bar{\phi}_{\mathrm{Ge}}(\omega)$ while $\bar{\phi}_{\mathrm{Te}}(\omega)$ exhibits a single

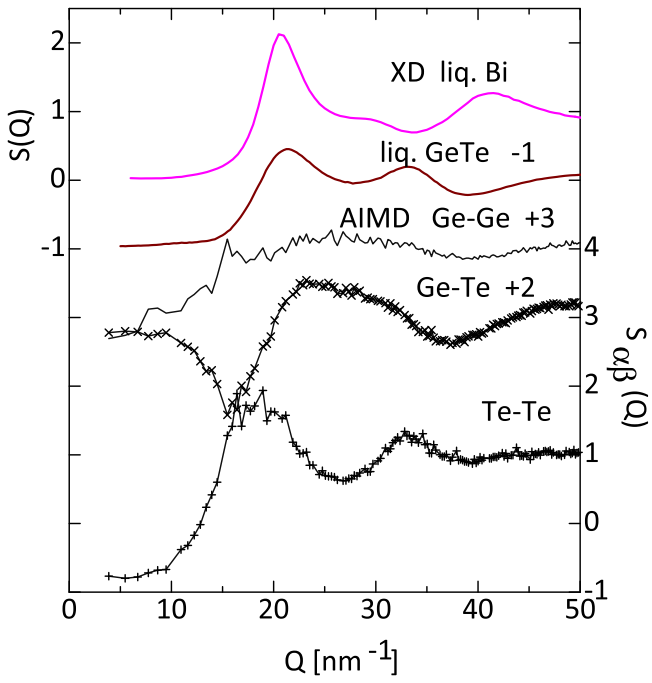

FIG. 9. Partial structure factors, $S_{\alpha\beta}(Q)$ (α,β = Ge,Te) obtained by the present AIMD. Also shown are $S_{\mathrm{XD}}(Q)$ of liquid Bi [23] and liquid GeTe [31]. For clarity, each curve is shifted by a value indicated in the figure.

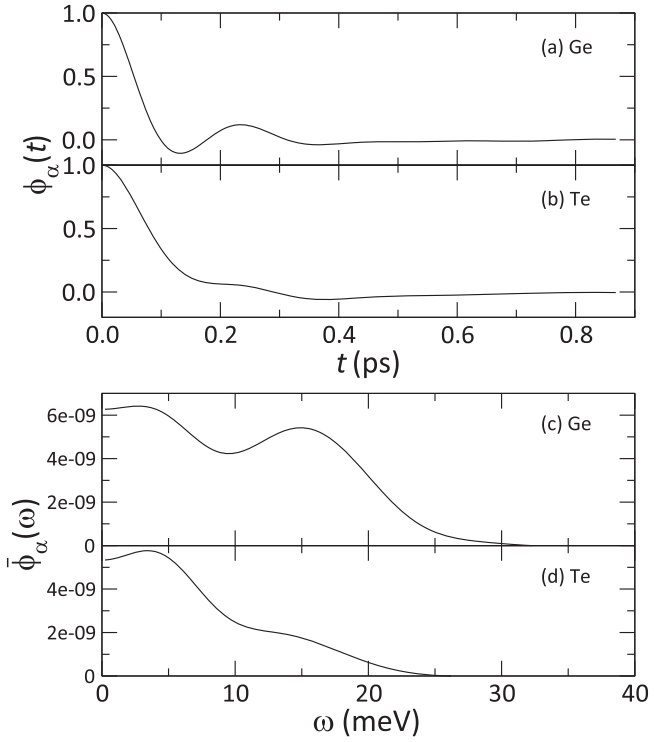

FIG. 10. The velocity autocorrelation functions and power spectra of Ge and Te atoms in liquid GeTe obtained by the present AIMD simulation. The unit of $\bar{\phi}_\alpha(\omega)$ is m^2/s.

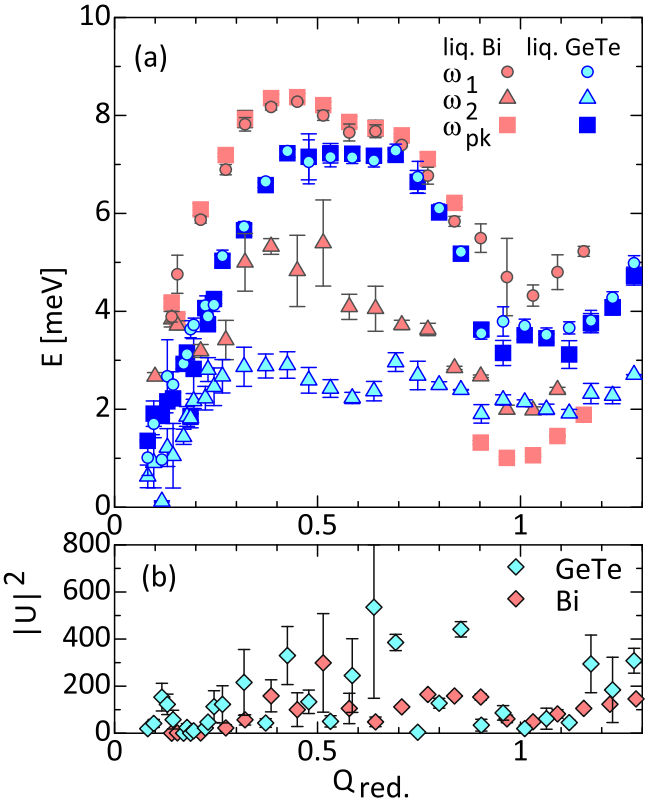

FIG. 11. (a) ω_1, ω_2, and ω_{pk} in liquid Bi [23] on a reduced Q scale. ω_1, ω_2, and ω_{pk} in liquid GeTe are normalized using the atomic mass of Bi and the reduced mass of GeTe. To obtain $Q_{red.}$, $Q_p = 20.7$ and 25.0 nm^{-1} were used for liquid Bi and liquid GeTe, respectively. (b) $|U|$ as a function of $Q_{red.}$.

maximum at 3 meV and a shoulder at 16 meV. The results suggest difference in single-particle dynamics between Ge and Te.

We compare $\bar{\phi}_\alpha(\omega)$ in liquid GeTe with that in liquid Bi obtained by AIMD simulations [22,36]. Crystalline Bi belongs to the $A7$ family, and the pair distribution of liquid Bi deduced from $S(Q)$ experimentally obtained could be related to $A7$-like local atomic configurations [37]. Ropo *et al.* [36] discussed that $\bar{\phi}(\omega)$ of liquid Bi is composed of diffusion and vibrational components. They assigned the lower energy part (<2 meV) as a gas phase or a diffusive one. As seen in Fig. 10, $\bar{\phi}_\alpha(\omega)$ of liquid GeTe seems to include a large amount of the diffusive component at low energy. The diffusion constants were approximately 6×10^{-9} and 5×10^{-9} m^2/s for Ge and Te, respectively, as indicated by the values on the ordinate. These constants were consistent with those deduced from the mean-square displacements in the present AIMD. The diffusion constant of Ge is larger than that of Te. This result is qualitatively consistent with that by Raty *et al.* [17]. They reported that the diffusion constant of Ge is a factor of 4 larger than that of Te. The large difference in the ratio between Raty *et al.* and ours may arise from differences in the simulation conditions. Their system size and density were, respectively, smaller and slightly larger than ours. Meanwhile, the simulation with a large system of 512 atoms [18] reports a self-diffusion constant of 2.3×10^{-9} m^2/s at 1128 K.

The bimodal profile of $\bar{\phi}_\alpha(\omega)$ in liquid GeTe is similar to $\bar{\phi}(\omega)$ in liquid Bi. Ropo *et al.* [36] concluded that a high-frequency vibrational mode at approximately 9 meV in $\bar{\phi}(\omega)$ corresponds to aspects of the crystalline structure in liquid Bi. Souto *et al.* [22] discussed a low-frequency excitation in $\bar{\phi}(\omega)$ obtained by their AIMD for liquid Bi, in the context of the previously mentioned approach by Gaskell and Miller [38], who developed a representation of $\phi(t)$ as sum of two contributions arising from the coupling of the single-particle motion to the collective longitudinal and transverse currents. According to these studies, a high-frequency vibrational mode at approximately 15 meV in liquid GeTe is coupled with the longitudinal-acoustic mode, and a large peak in $\bar{\phi}_{Ge}(\omega)$ indicates that Ge atoms contribute to the longitudinal motion more frequently than Te atoms. Note that the maximum energy of the longitudinal-acoustic excitation obtained by the IXS is also approximately 15 meV. Meanwhile, a distinct low-frequency vibrational mode at approximately 4 meV in $\bar{\phi}_\alpha(\omega)$ indicates that a transverse-acoustic mode is excited in liquid GeTe.

C. Collective dynamics

First we describe the results of liquid Bi obtained by the present analysis for the IXS data reported in [23]. $S(Q,E)/S(Q)$ of liquid Bi were well reproduced by 2-IO. χ^2/N and Bayesian analysis indicated that 2-IO model is superior to 2-DHO model in liquid Bi at $Q \geqslant 2.9$ nm^{-1}. Figure 11(a) shows ω_1 (light red circles), ω_2 (light red triangles), and ω_{pk} (light red squares) of liquid Bi as a function of a reduced Q, $Q_{red.} = Q/Q_p$. Strong softening of ω_{pk} occurs

at $Q_{\text{red.}} = 1$ in liquid Bi. The present analysis shows that a flat-topped dispersion curve of ω_{pk} in liquid Bi is less clearly visible compared to the previous one [23]. As shown in Fig. 11(b), U (light red diamonds) took a large value at $0.4 \leqslant Q_{\text{red.}} \leqslant 0.9$. The result suggests that a coupling between the longitudinal-acoustic and low-frequency modes becomes strong at Q where a dispersion curve deviates from a sinusoidal curve. The dispersion curve of ω_2 in liquid Bi is steep up to $Q_{\text{red.}} = 0.4$. In the previous study [23], although a lower excitation energy in liquid Bi was expected to originate from the transverse-acoustic mode, 2-DHO could not be applied to the data at $Q \leqslant 6$ nm^{-1}. In the present analysis, 2-IO could reveal the dispersion curve of the lower excitation energy at $2.9 \leqslant Q < 6$ nm^{-1}. However, ω_2 was much higher than the transverse-acoustic excitation energies predicted by the AIMD simulation for liquid Bi [36].

To compare the acoustic dispersion curve of liquid GeTe with that of liquid Bi, differences in the atomic mass and size should be taken into account. We normalized the excitation energies of liquid GeTe with a square root of the ratio of Bi atomic mass to GeTe reduced mass. To normalize Q, we investigated the average hard sphere diameter D in liquid GeTe because in monatomic systems, a normalization QD is often used. As shown in Fig. 7, Te-Te pairs in $g_{\text{TeTe}}(r)$ hardly contribute to the first coordination shell. When D is regarded as the first peak position in $g_{\alpha\beta}(r)$, r_{GeGe} and r_{GeTe} are 0.267 and 0.278 nm, respectively. These distances are approximately consistent with 0.257 and 0.274 nm reported in Ref. [18]. Although Q values corresponding to these distances $(2\pi/D)$ are slightly smaller than 25 nm^{-1}, the mean value of a broad maximum in $S_{\text{GeGe}}(Q)$ and $S_{\text{GeTe}}(Q)$ is approximately 25 nm^{-1} where ω_1 and ω_{pk} exhibit minima as shown in Fig. 5. Hence, we calculated $Q_{\text{red.}}$ using $Q_{\text{p}} = 25$ nm^{-1} for the results of liquid GeTe.

We plot normalized ω_1 (light blue circles), ω_2 (light blue triangles), and ω_{pk} (blue squares) of liquid GeTe as a function of $Q_{\text{red.}}$ in Fig. 11(a). Softening of ω_{pk} is observable at $Q_{\text{red.}} = 1$ in both of liquid Bi and liquid GeTe. At $Q_{\text{red.}} \leqslant 0.4$, ω_{pk} of liquid Bi (light red squares) disperses faster than ω_{pk} of liquid GeTe (blue squares). Normalized ω_{pk} in liquid GeTe stay at approximately constant energies at $0.4 \leqslant Q_{\text{red.}} \leqslant 0.7$ and its maximum value is approximately 7 meV, which is lower than ω_{pk} in liquid Bi. The result does not indicate that normalization with atomic mass cannot provide a reduced interatomic interaction common between these liquids. In fact, the nearest-neighbor coordination number in liquid Bi [22] is larger than that in liquid GeTe. Also from this difference in a local atomic configuration, it is expected that the interatomic interaction cannot be reduced between these liquids.

The optimized U of liquid GeTe (light blue diamonds) becomes large at $Q_{\text{red.}} = 0.4$ and $Q_{\text{red.}} = 0.7$, both ends of the flat-topped region of ω_{pk}, as shown in Fig. 11(b). The result suggests that a coupling between the longitudinal-acoustic mode and low-energy excitations is responsible to make a unique dispersion profile. Hence, it is reasonable to consider that the low-energy excitations in $S(Q,E)/S(Q)$ of liquid GeTe arises from mixing of the longitudinal and transverse-acoustic modes, as reported in Ref. [39]. The $A7$-like local structure, especially expected around a central Ge atom, may promote such a coupling in liquid GeTe.

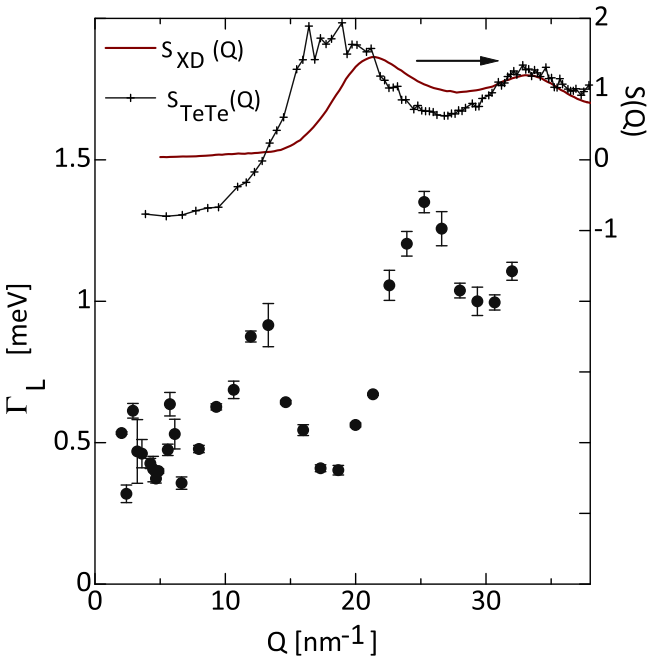

FIG. 12. Q dependence of Γ_{L} obtained by 2-IO at $Q \geqslant 3$ nm^{-1}. Γ_{L} at $Q < 3$ nm^{-1} is a 1-DHO result. Also shown is $S_{\text{XD}}(Q)$ [31] and $S_{\text{TeTe}}(Q)$.

Recently, Bryk and Wax [40] reported that the attribute of a low-energy excitation to a transverse-acoustic atomic motion is suspect in a simple liquid metal, based on their AIMD simulation for liquid Na. Liquid GeTe is, however, classified as a nonsimple liquid with asymmetrical local structure due to the Peierls distortion. ω_2 in Fig. 5 stays at $E \leqslant 7$ meV and a low-frequency mode is clearly observed at $\omega \leqslant 7$ meV in $\overline{\phi}_{\alpha}(\omega)$ in Fig. 10. These results again support that ω_2 in liquid GeTe originates from a transverse-acoustic atomic motion.

Finally we present de Gennes narrowing behavior in liquid GeTe. Figure 12 shows Γ_{L}, the quasielastic linewidth, as a function of Q. The figure also plots $S_{\text{XD}}(Q)$ and $S_{\text{TeTe}}(Q)$. Γ_{L} exhibits a clear minimum at 18 nm^{-1} slightly lower than Q_{p} in $S_{\text{XD}}(Q)$. Such a behavior that the minimum of the quasielastic linewidth shifts from Q_{p} is inconsistent with the idea by de Gennes for a simple liquid [41]. In practice, the minimum of the quasielastic linewidth coincides with Q_{p} in liquid Bi [42]. As another example of a monatomic liquid, inconsistency between the minimum position of the quasielastic linewidth and Q_{p} was reported by an IXS study on liquid Si [43]. In the case of liquid GeTe, however, the minimum position of Γ_{L} coincides with the first peak position in $S_{\text{TeTe}}(Q)$. This implies that the quasielastic component in $S(Q,E)/S(Q)$ of liquid GeTe is largely dominated by Te-Te correlation. Very small vibrational intensity at 15 meV in $\overline{\phi}_{\text{Te}}(\omega)$ and weak diffusive behavior of Te compared to Ge seem to be correlated with this result.

VI. SUMMARY

IXS measurements for liquid GeTe revealed that the longitudinal-acoustic dispersion curve exhibits a flat-topped profile similar to that recently observed in liquid Bi. An interacting oscillator (IO) model clarified that a coupling between

the longitudinal-acoustic and low-frequency modes makes an important contribution to peculiar dispersion curves observed in both liquids. Low-energy excitations in $S(Q,E)/S(Q)$ of liquid GeTe appear near the energy of a low-frequency vibrational mode in $\overline{\phi}_\alpha(\omega)$ that is expected to originate from transverse-acoustic excitations. From these results, we concluded that the low-energy excitations arise from mixing of the longitudinal- and transverse-acoustic modes. We interpret that the mixings are correlated with asymmetrical bonding, as is also seen in the solid $A7$ crystalline phases of both materials.

The results of the AIMD simulations [17,18,24] could advance the analysis of atomic dynamics in liquid GeTe obtained by IXS. By comparing Q dependence of excitation energies experimentally obtained with partial structure factors obtained by AIMD, we demonstrated that the flat-topped dispersion curve is strongly affected by Ge-Ge and Ge-Te correlations. From the AIMD result that the atomic configuration at a Ge site has more $A7$-like order than at a Te site [24], it is inferred that alternation of shorter and longer bonds in a distorted simple cubic configuration promotes a coupling between the longitudinal and transverse-acoustic modes. The AIMD simulations show that a Te-Te correlation has small population at the first coordination shell. From the result that the quasielastic linewidth exhibits a minimum at Q where $S_{\mathrm{TeTe}}(Q)$ has the first maximum, we concluded that a Te-Te correlation largely contributes to the quasielastic component in $S(Q,E)/S(Q)$ of liquid GeTe. The result is consistent with a single-particle property obtained by the AIMD: the diffusion constant of Te is smaller than that of Ge.

ACKNOWLEDGMENTS

The authors would like to thank S. Kohara for supplying $S_{\mathrm{XD}}(Q)$ data of liquid GeTe [31] and valuable discussion. The authors would like to acknowledge Japan Society for the Promotion of Science (JSPS) for a Grant-in-Aid for Scientific Research for a Grant-in-Aid for Scientific Research (A) (Grant No. 20244061) and (B) (Grant No. 23340106). The synchrotron radiation experiments were performed at the SPring-8 with the approval of the Japan Synchrotron Radiation Research Institute (JASRI) (Proposals No. 2013B1269, No. 2013B1268, and No. 2012A1354).

[1] R. J. Huck and E. A. Johnson, Phys. Rev. Lett. **44**, 142 (1980).
[2] J. Bosse, G. Jacucci, M. Ronchetti, and W. Schirmacher, Phys. Rev. Lett. **57**, 3277 (1986).
[3] A. Campa and E. G. D. Cohen, Phys. Rev. Lett. **61**, 853 (1988).
[4] P. H. K. de Jong, P. Verkerk, C. F. de Vroege, L. A. de Gaaf, W. S. Howells, and S. M. Bennington, J. Phys.: Condens. Matter **6**, L681 (1994).
[5] T. Bryk and J.-F. Wax, Phys. Rev. B **80**, 184206 (2009).
[6] J.-P. Hansen, I. R. McDonald, and E. L. Pollock, Phys. Rev. A **11**, 1025 (1975).
[7] J.-P. Hansen and I. R. McDonald, Phys. Rev. A **11**, 2111 (1975).
[8] E. M. Adams, I. R. McDonald, and K. Singer, Proc. R. Soc. London, Ser. A **357**, 37 (1977).
[9] M. Dixon, Philos. Mag. B **47**, 531 (1983).
[10] R. L. McGreevy and E. W. J. Mitchell, J. Phys. C **15**, L1001 (1982).
[11] R. L. McGreevy, Solid State Phys. **40**, 247 (1987).
[12] F. J. Bermejo, J. W. Taylor, S. E. McLain, I. Bustinduy, J. F. C. Turner, M. D. Ruiz-Martin, C. Cabrillo, and R. Fernandez-Perea, Phys. Rev. Lett. **96**, 235501 (2006).
[13] T. Bryk and I. Mryglod, Phys. Rev. B **79**, 184206 (2009).
[14] S. Hosokawa, M. Inui, T. Bryk, I. Mryglod, F. Demmel, W.-C. Pilgrim, Y. Kajihara, K. Matsuda, M. Yao, Y. Ohmasa, S. Tsutsui, and A. Q. R. Baron, in *Abstracts of 14th Liquid and Amorphous Materials Conference*, Rome, 11-16 July 2010 (University of Rome, Rome, 2010), p. 240, http://arxiv.org/abs/1801.04196.
[15] R. E. Peierls, in *Quantum Theory of Solids* (Oxford University Press, Oxford, New York, 1955), p. 108.
[16] R. Bellissent, C. Bergman, R. Ceolin, and J. P. Gaspard, Phys. Rev. Lett. **59**, 661 (1987).
[17] J. Y. Raty, V. V. Godlevsky, J. P. Gaspard, C. Bichara, M. Bionducci, R. Bellissent, R. Ceólin, J. R. Chelikowsky, and Ph. Ghosez, Phys. Rev. B **65**, 115205 (2002).
[18] H. Weber, M. Schumacher, P. Jóvári, Y. Tsuchiya, W. Skrotzki, R. Mazzarello, and I. Kaban, Phys. Rev. B **96**, 054204 (2017).
[19] A. Q. R. Baron, Y. Tanaka, S. Goto, K. Takeshita, T. Matsushita, and T. Ishikawa, J. Phys. Chem. Solids **61**, 461 (2000).
[20] M. Zanatta, F. Sacchetti, E. Guarini, A. Orecchini, A. Paciaroni, L. Sani, and C. Petrillo, Phys. Rev. Lett. **114**, 187801 (2015).
[21] M. Zanatta, A. Fontana, A. Orecchini, C. Petrillo, and F. Sacchetti, J. Phys. Chem. Lett. **4**, 1143 (2013).
[22] J. Souto, M. M. G. Alemany, L. J. Gallego, L. E. González, and D. J. González, Phys. Rev. B **81**, 134201 (2010).
[23] M. Inui, Y. Kajihara, S. Munejiri, S. Hosokawa, A. Chiba, K. Ohara, S. Tsutsui, and A. Q. R. Baron, Phys. Rev. B **92**, 054206 (2015).
[24] A. Koura and F. Shimojo, EPJ Web Conf. **151**, 01002 (2017).
[25] K. Tamura, M. Inui, and S. Hosokawa, Rev. Sci. Instrum. **70**, 144 (1999).
[26] Y. Tsuchiya, J. Phys. Soc. Jpn. **60**, 227 (1991).
[27] M. Inui, Y. Kajihara, K. Matsuda, S. Hosokawa, K. Tamura, M. Yao, Y. Tsuchiya, D. Ishikawa, S. Tsutsui, and A. Q. R. Baron, Eur. Phys. J.: Spec. Top. **196**, 167 (2011).
[28] G. Kresse and J. Hafner, Phys. Rev. B **49**, 14251 (1994).
[29] F. Shimojo, R. K. Kalia, A. Nakano, and P. Vashishta, Comput. Phys. Commun. **140**, 303 (2001).
[30] *International Tables for X-ray Crystallography*, edited by K. Lonsdale (Kynoch, Birmingham, 1974), Vol. IV, Table 2.2B.
[31] S. Kohara, K. Kato, S. Kimura, H. Tanaka, T. Usuki, K. Suzuya, H. Tanaka, Y. Moritomo, T. Matsunaga, N. Yamada, Y. Tanaka, H. Suematsu, and M. Takata, Appl. Phys. Lett. **89**, 201910 (2006).
[32] D. N. Zubarev, Sov. Phys. Usp. **3**, 320 (1960).
[33] R. J. Elliott, J. A. Krumhansl, and P. L. Leath, Rev. Mod. Phys. **46**, 465 (1974).
[34] B. Fåk and B. Dorner, Physica B (Amsterdam) **234–236**, 1107 (1997).
[35] D. S. Sivia and J. Skilling, *Data Analysis, A Bayesian Tutorial*, 2nd ed. (Oxford University Press, Oxford, UK, 2006).

[36] M. Ropo, J. Akola, and R. O. Jones, J. Chem. Phys. **145**, 184502 (2016).
[37] M. Mayo, E. Yahel, Y. Greenberg, and G. Makov, J. Phys.: Condens. Matter **25**, 505102 (2013).
[38] T. Gaskell and S. Miller, J. Phys. C **11**, 3749 (1978).
[39] S. Hosokawa, S. Munejiri, M. Inui, Y. Kajihara, W.-C. Pilgrim, Y. Ohmasa, S. Tsutsui, A. Q. R. Baron, F. Shimojo, and K. Hoshino, J. Phys.: Condens. Matter **25**, 112101 (2013).
[40] T. Bryk and J.-F. Wax, J. Chem. Phys. **144**, 194501 (2016).
[41] P. G. de Gennes, Physica **25**, 825 (1959).
[42] M. Inui, Y. Kajihara, S. Munejiri1, S. Hosokawa, A. Chiba, K. Ohara, S. I. Tsutsui, and A. Q. R. Baron, EPJ Web Conf. **151**, 06001 (2017).
[43] S. Hosokawa, W.-C. Pilgrim, Y. Kawakita, K. Ohshima, S. Takeda, D. Ishikawa, S. Tsutsui, Y. Tanaka, and A. Q. R. Baron, J. Phys.: Condens. Matter **15**, L623 (2003).